

A New Treatment of the Coriolis Terms in C-Grid Models at Both High and Low Resolutions

A. J. ADCROFT, C. N. HILL, AND J. C. MARSHALL

*Department of Earth, Atmospheres and Planetary Science, Massachusetts Institute of Technology,
Cambridge, Massachusetts*

12 January 1998 and 9 December 1998

ABSTRACT

Numerical models of the ocean typically employ gridpoint techniques in which the dynamical variables defining the state of the ocean are held on a staggered grid. One common arrangement of the variables, known as the Arakawa C-grid, is particularly prone to gridscale noise that is due to spatial averaging of Coriolis terms and that is manifest when the grid resolution is coarse with respect to the deformation radius. Here, the authors analyze the problem in the context of linear inertia-gravity waves and discuss the reason for the prevalence of noise. They suggest a solution to the problem in which the C-grid model variables are augmented with D-grid velocity variables. An analysis of the resulting C-D grid indicates favorable behavior and numerical results are presented to demonstrate this. Finally, they discuss the similarity in nature between the C-D grid and the Z-grid, to explain why the C-D grid works well at both high and low resolution.

1. Introduction

Models of ocean circulation typically employ gridpoint techniques in which the variables defining the state of the ocean (velocity components, temperature, salinity, and pressure) are held on a staggered grid. The most common grids employed in ocean models are the B-, C-, and E-grids [in the nomenclature of Arakawa and Lamb (1977)]. Linear analysis of the representation of inertia-gravity waves on each grid shows the C-grid to have the most satisfactory properties; provided the grid resolution is high relative to the deformation radius. However, since the deformation radius in the ocean is only 30 km or so, most global (and even regional) ocean models coarsely resolve the radius of deformation. The conventional formulation of Coriolis terms in a C-grid model involves spatial averaging because the horizontal components of velocity, u and v , are staggered in space. This averaging allows gridscale noise to persist in the divergence of u and v and hence, in the vertical velocity field. For example Fig. 1a shows the vertical velocity in the Massachusetts Institute of Technology (MIT) ocean model (Marshall et al. 1997) after only a brief period of spinup from rest. The model shown here is a full three-dimensional general circulation model with realistic topography and forcing that employs just a conventional C-grid for the horizontal discretization. The

noise, as seen at this early stage in the integration, is generated at boundaries and over topography and then rapidly propagates into the interior of the model. As the integration proceeds matters become worse with intolerable levels of noise. The prevalence of noise can be traced back directly to the discretization of the Coriolis force. This problem does not arise in B-grid models, where u and v are collocated (Bryan 1969; Mesinger and Arakawa 1976).

When the deformation radius is well resolved, C-grid models yield the most accurate numerical solutions. Consequently, many ocean models based on the C-grid have been developed for use at high resolutions (e.g., Smith et al. 1990; Haidvogel et al. 1991; Blanke and Delecluse 1993; Marshall et al. 1997). In subsequent attempts to apply such models to large-scale and global simulations at low resolution they have proved susceptible to gridscale noise. This is, in part, because there are many potential sources of gridscale energy, among them flow over topography that can vary rapidly from grid point to grid point. Several "fixes" to deal with the noise have been proposed and are frequently employed. Most involve some form of higher-order, scale-selective dissipation that aggressively damps gridscale phenomena, thus papering over the problem at the expense of accurate dynamics. For example, one such method is "divergence damping" (Smith et al. 1990); here terms are added to the momentum equations that damp only the divergent part of the flow. Divergence damping presumes that the important dynamics are in the rotational flow, which is not necessarily true, especially at low latitudes.

Corresponding author address: Dr. Alistair J. Adcroft, MIT 54-1523, 77 Massachusetts Ave., Cambridge, MA 02139.
E-mail: adcroft@mit.edu

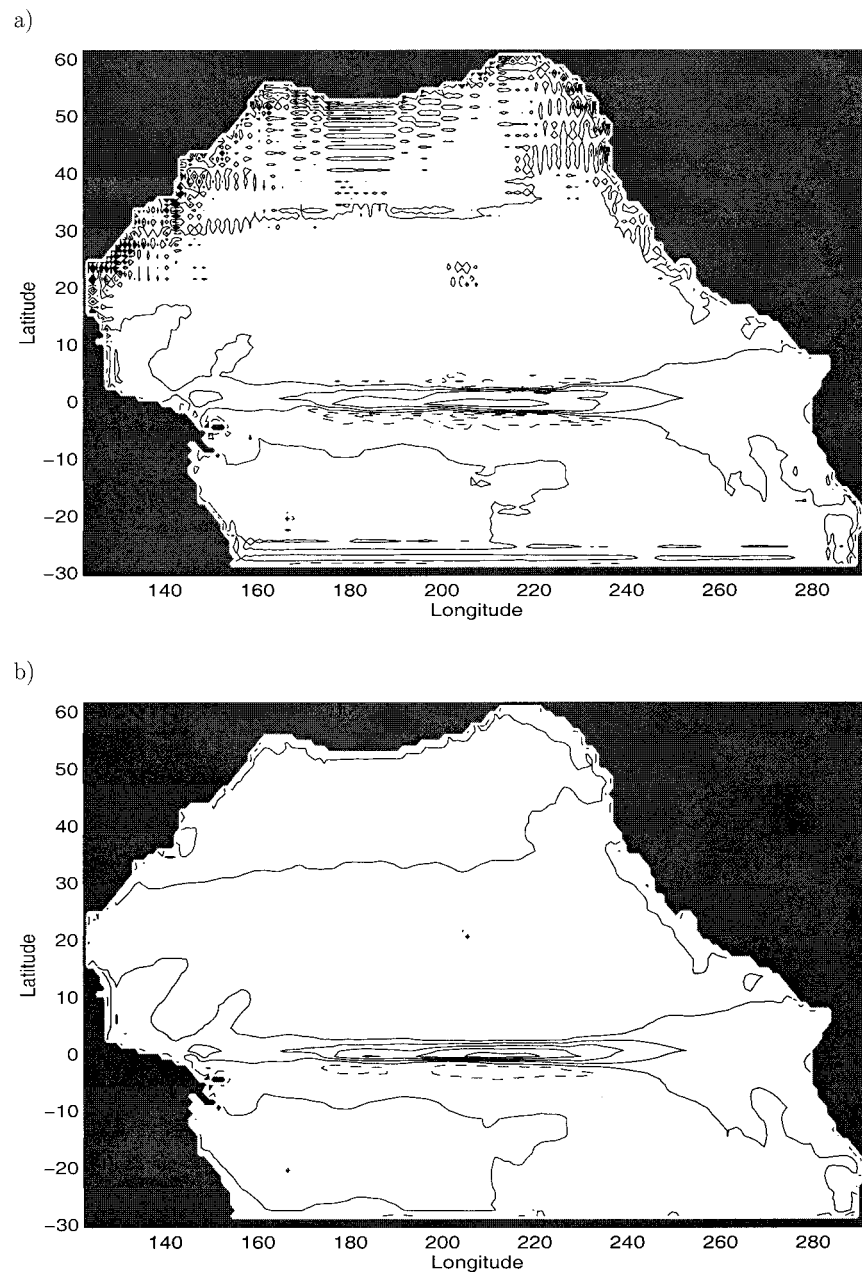


FIG. 1. The vertical velocity field at $z = -25$ m in two three-dimensional models of the Pacific basin after one month of spinup. They solve the primitive equations on the sphere on (a) the C-grid and (b) the C-D grid. The models use realistic topography and forcing. Contour interval is 0.01 mm s^{-1} .

In this note we reassess the conventional formulation of Coriolis terms on the C-grid and suggest a new approach which involves augmenting the C-grid velocities with those from a D-grid. The resulting grid, which we call C-D, yields satisfying results at both fine and coarse resolution—see, for example, Fig. 1b in which we have implemented the MIT ocean model on the C-D grid. Moreover, this approach can readily be switched back to a C-grid for use at high resolution. In section 2 we

discuss the essence of the C-grid problem. We suggest the C-D grid as an alternative and describe the approach in section 3. We then test the C-D grid side-by-side with C-grid and B-grid models in section 4.

2. Inertia-gravity waves on the C-grid

Consider the following second-order discretization of the linear shallow water equations on a C-grid:

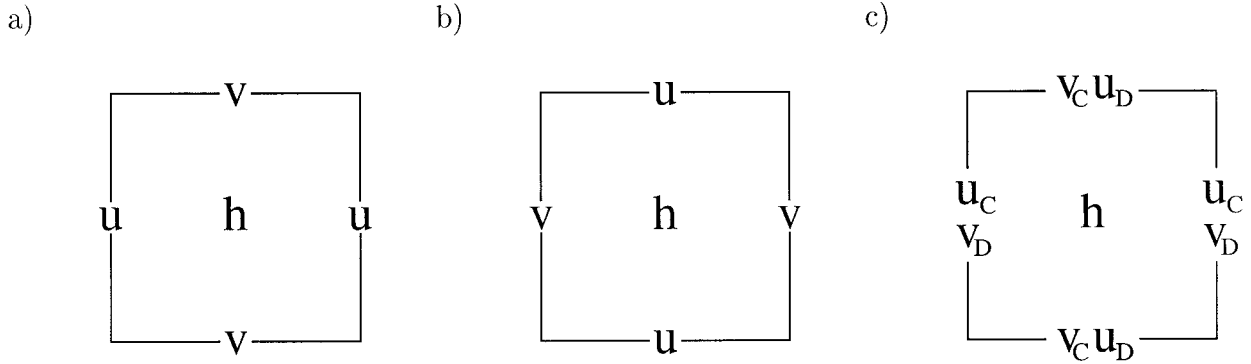


FIG. 2. The spatial arrangement of variables on (a) the C-grid, (b) the D-grid, and (c) the C-D grid. Note that the number of velocity variables per pressure point on the C-D grid is twice that of the C- or D-grid.

$$\frac{1}{\Delta t} \delta_t u - f \bar{v}^{xyt} + \frac{g'}{\Delta x} \delta_x h = 0$$

$$\frac{1}{\Delta t} \delta_t v + f \bar{u}^{xyt} + \frac{g'}{\Delta y} \delta_y h = 0$$

$$\frac{1}{\Delta t} \delta_t h + H_o \left(\frac{1}{\Delta x} \delta_x u + \frac{1}{\Delta y} \delta_y v \right) = 0.$$

Here, $(1/\Delta t)\delta_t$, $(1/\Delta x)\delta_x$, and $(1/\Delta y)\delta_y$ are the centered discrete operators that approximate the continuous partial derivatives ∂_t , ∂_x , and ∂_y , respectively (e.g., $\delta_x u = u(t + \Delta t/2) - u(t - \Delta t/2)$). The $-t$, $-x$, and $-y$ operators are, respectively, centered in time and in the x and y directions (e.g., $\bar{u}^t = \frac{1}{2}[u(t - \Delta t/2) + u(t + \Delta t/2)]$). Figure 2a shows the spatial layout of variables on the C-grid. Note that the Coriolis terms are centered in time by use of the $-t$ operator, required because u and v are both evaluated at the same time level. The pressure term is staggered in time with respect to the velocity (see Fig. 3 for temporal discretisation) allowing $g'\nabla h$ and $H_o \nabla \cdot \mathbf{v}$ to be time centered and explicit.

To analyze the gravity waves in the above system, we assume a simple wave solution of form $e^{i(kx+ly-\omega t)}$. On substitution into the unforced, inviscid system we obtain the discrete dispersion relation

$$s_\omega^2 = f^2 c_k^2 c_l^2 c_\omega^2 + g' H_o (s_k^2 + s_l^2), \tag{1}$$

where

$$s_\omega = \frac{2}{\Delta t} \sin \frac{\omega \Delta t}{2},$$

$$s_k = \frac{2}{\Delta x} \sin \frac{k \Delta x}{2},$$

$$s_l = \frac{2}{\Delta y} \sin \frac{l \Delta y}{2},$$

$$c_\omega = \cos \frac{\omega \Delta t}{2},$$

$$c_k = \cos \frac{k \Delta x}{2},$$

and

$$c_l = \cos \frac{l \Delta y}{2}.$$

In the limit of infinitesimal time step, $\Delta t \rightarrow 0$, and grid spacing, $\Delta x \rightarrow 0$ and $\Delta y \rightarrow 0$, then the trigonometric quantities become $s_\omega \rightarrow \omega$, $s_k \rightarrow k$, $s_l \rightarrow l$, $c_\omega \rightarrow 1$, $c_k \rightarrow 1$, and $c_l \rightarrow 1$ and the discrete inertia-gravity modes (1) asymptote to the more familiar continuum modes

$$\omega^2 = f^2 + g' H_o (k^2 + l^2). \tag{2}$$

The form of the discrete dispersion relation (1) determines the behavior of inertia-gravity waves in the discrete model. The behavior is characterized by the *wave resolution*, r , defined as

$$r \equiv 2 \frac{L_p}{\Delta x} = 2 \frac{\sqrt{g' H_o}}{f \Delta x}.$$

There are two regimes of behavior: (i) low resolution, $r < 1$, where the frequency is dominated by the Coriolis frequency since all wavelengths permitted on the grid are long relative to the deformation radius, and (ii) high resolution, $r > 1$, where the waves are more dispersive. Figure 4 shows the nondimensional frequency ω/f for

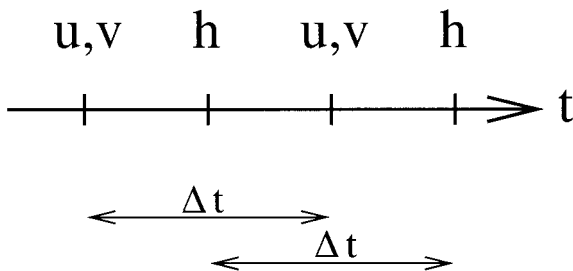


FIG. 3. The arrangement of variables on the timeline. The velocity variables are staggered with respect to the pressure. This allows the pressure term ($g'\nabla h$) to coincide with the acceleration ($\delta_x u$) and the horizontal divergence ($H_o \nabla \cdot \mathbf{u}$) to coincide with the vertical velocity ($\delta_y h$).

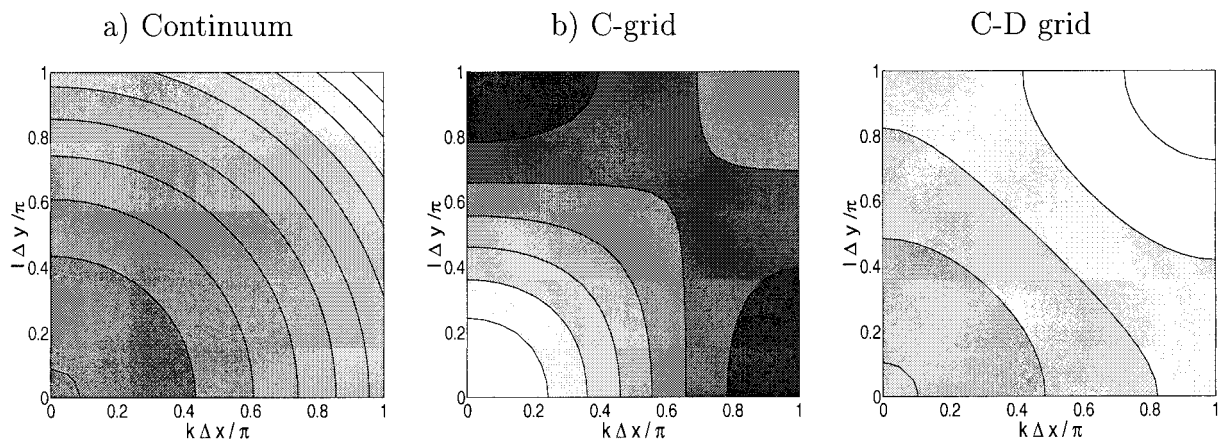
Low resolution ($r = 0.2$)

FIG. 4. Inertia-gravity wave frequency in the “low”-resolution ($r = \frac{1}{2}$) regime. The nondimensional frequency ω/f is contoured for (a) the continuum, (b) the C-grid, and (c) the C-D grid. A contour interval of 0.05 is used for all plots.

(a) the continuum and (b) the C-grid, both in the low-resolution regime ($r = \frac{1}{2}$). The C-grid exhibits false minima that are not present in the continuum. The false minima are due to the presence of the factor $c_k c_l$ in the dispersion relation. Here, $c_k c_l$ causes the inertial oscillation term (f^2) to vanish for waves with either $k = \pi/\Delta x$ and/or $l = \pi/\Delta y$. These conditions correspond to long/short-meridional and short/long-zonal structures that describe the patterns of noise seen in the GCM calculation, Fig. 1a. The false minima also mean that the group velocity has an incorrect sign for some waves. In a well-behaved system, perturbations on the gridscale would adjust to balanced flow through the transmission of energy by inertia-gravity waves. Instead, on the C-grid, gridscale waves feed energy into short-scale per-

turbations thus allowing standing gridscale noise to persist. Figure 5 shows ω/f for (a) the continuum and (b) the C-grid, both for a wave resolution of $r = 2$ (i.e., in the high-resolution regime). The structure of the C-grid dispersion relation resembles more closely that of the continuum. There are no false minima and the frequency increases monotonically with wavenumber.

The conventional wisdom, then, is that the C-grid is well behaved in the limit of high resolution ($r > 1$) but is prone to gridscale noise at the low resolution ($r < 1$). This property can be traced back to the spatial averaging of the Coriolis terms on the C-grid. More comprehensive analyses of the adjustment process can be found in Arakawa and Lamb (1977) and Fox-Rabinovitz (1991) and a further analyses for Kelvin and Rossby

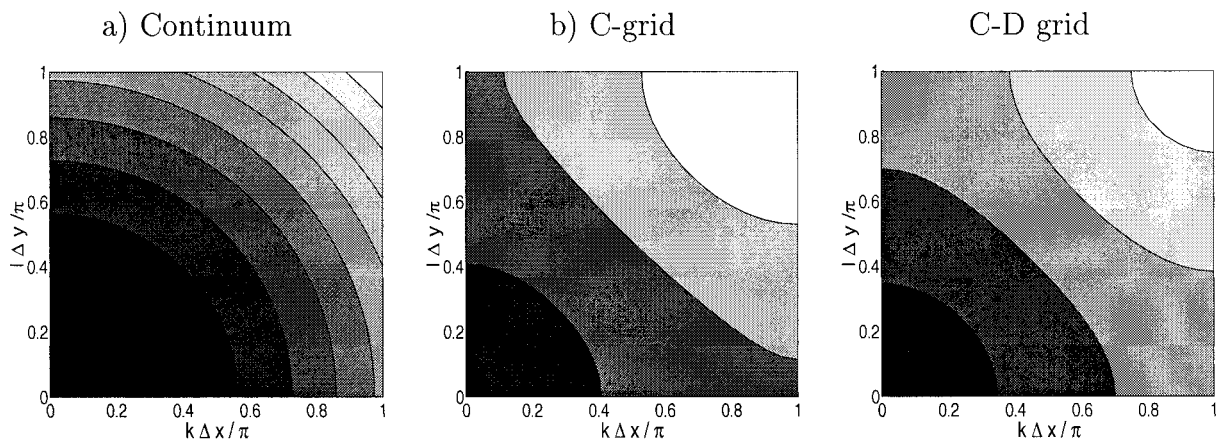
High resolution ($r = 2$)

FIG. 5. Inertia-gravity wave frequencies in the “high”-resolution ($r = 2$) regime. Here, ω/f is contoured for (a) the continuum, (b) the C-grid, and (c) the C-D grid. A contour interval of 0.1 is used for all plots.

waves, not discussed here, can be found in Wajsovicz and Gill (1986a,b,c).

3. The C–D grid

The existence of false minima in the discrete dispersion relation (1) is a consequence of the spatial averaging of the Coriolis terms on the C-grid. Spatial averaging leads to cosines ($c_k^2 c_l^2$) that multiply the Coriolis frequency in the dispersion relation and that tend to zero for gridscale wavelengths. If this averaging can be avoided, the dispersion relation will be improved.

One way forward, and this is the contribution of the present note, is to employ a combination of the C- and D-grids. On overlaying the C-grid (Fig. 2a) and D-grid (Fig. 2b) such that the pressure points in the respective grids are aligned, we obtain the spatial distribution of model variables depicted in Fig. 2c. We label the velocity variables with subscripts according to the subgrid (C or D) with which they are associated. The second-order discretization, centered in space and time, of the linear inertia–gravity wave terms for this C–D grid is

$$\frac{1}{\Delta t} \delta_t u_C - f \overline{v_D}^t + \frac{g'}{\Delta x} \delta_x h = 0, \quad (3a)$$

$$\frac{1}{\Delta t} \delta_t v_C + f \overline{u_D}^t + \frac{g'}{\Delta y} \delta_y h = 0, \quad (3b)$$

$$\frac{1}{\Delta t} \delta_t h + H_o \left(\frac{1}{\Delta x} \delta_x u_C + \frac{1}{\Delta y} \delta_y v_C \right) = 0, \quad (3c)$$

$$\frac{1}{\Delta t} \delta_t u_D - f \overline{v_C}^t + \frac{g'}{\Delta x} \delta_x \overline{h}^{xy} = 0, \quad (3d)$$

and

$$\frac{1}{\Delta t} \delta_t v_D + f \overline{u_C}^t + \frac{g'}{\Delta y} \delta_y \overline{h}^{xy} = 0. \quad (3e)$$

The first three equations are the same as in a conventional C-grid discretization except for the Coriolis terms where we have used the D-grid velocities that require no interpolation. The last two equations can then be viewed as auxiliary to that of the C-grid model required to predict the velocities for use in the C-grid Coriolis terms. Note that the D-grid equations [(3d) and (3e)] are only required in the interior because the Coriolis terms in (3a) and (3b) are not evaluated on the boundary. Again, assuming a wave solution we obtain five modes that are

$$s_\omega = 0, \quad (4a)$$

$$s_\omega^2 = f^2 c_\omega^2 + g' H (s_k^2 + s_l^2), \quad (4b)$$

and

$$s_\omega^2 = f^2 c_\omega^2. \quad (4c)$$

The first mode (4a) is the geostrophic mode; on a β -plane it would be a planetary Rossby wave. The mid-

dle pair of modes (4b) are inertia–gravity waves and the last pair (4c) are computational modes. These computational modes are a consequence of using twice as many velocity variables as on the C-grid alone. Note that there is no spatial averaging in the dispersion relation of the inertia–gravity waves on the C–D grid (4b). The right-hand side is monotonic in k and l implying the sense of the group velocity is always faithful to that of the continuum, independent of spatial resolution (Figs. 4c and 5c). This is also a feature of the E-grid, Eliassen grid, and Z-grid (see discussion Randall 1994). The dispersion of inertia–gravity waves is therefore now “properly” modeled in that energy is not transmitted in the wrong direction. This indicates the gridscale noise will not persist as standing patterns, unlike in a pure C-grid model, as will be demonstrated later in a numerical C–D model.

Filtering the computational modes

The computational modes on the C–D grid take the form of inertial oscillations and have no particular spatial characteristics. They can readily be filtered by use of an implicit time-stepping technique. In the previous section we used a Crank–Nicholson time-stepping scheme, yielding Coriolis terms that were centered and implicit in time. If we now replace the Crank–Nicholson method with an implicit backward scheme, then the inertial oscillations will be damped, together with the computational modes. Damping is not the same as dissipation; additional dissipation would alter the balanced state whereas here, only the transients about the balanced state are damped. We will now describe in detail how this is achieved.

The C–D discrete equations, using a general time-stepping scheme for the Coriolis terms and now including forcing and dissipation, can be written as

$$\frac{1}{\Delta t} \delta_t u_C - f \widetilde{v_D}^t + \frac{g'}{\Delta x} \delta_x h = \tau^{(x)} - \epsilon u_C, \quad (5a)$$

$$\frac{1}{\Delta t} \delta_t v_C + f \widetilde{u_D}^t + \frac{g'}{\Delta y} \delta_y h = \tau^{(y)} - \epsilon v_C, \quad (5b)$$

$$\frac{1}{\Delta t} \delta_t h + H \left(\frac{1}{\Delta x} \delta_x u_C + \frac{1}{\Delta y} \delta_y v_C \right) = 0, \quad (5c)$$

$$\frac{1}{\Delta t} \delta_t u_D - f \widetilde{v_C}^t + \frac{g'}{\Delta x} \delta_x \overline{h}^{xy} = \overline{\tau^{(x)}}^{xy} - \epsilon u_D, \quad (5d)$$

and

$$\frac{1}{\Delta t} \delta_t v_D + f \widetilde{u_C}^t + \frac{g'}{\Delta y} \delta_y \overline{h}^{xy} = \overline{\tau^{(y)}}^{xy} - \epsilon v_D, \quad (5e)$$

where the tilde operator is defined as

$$\widetilde{u}^t = \alpha u(t + \Delta t/2) + (1 - \alpha) u(t - \Delta t/2),$$

and α is a time-weighting factor. For $\alpha = 0, 1/2$, and 1 we obtain, respectively, the Euler forward, Crank–Nich-

olson, and implicit backward time-stepping schemes for the Coriolis terms. Note that the velocities and pressure remain staggered in time ensuring that the gravity wave terms are centered, second-order accurate in time, and can be evaluated explicitly.

A stability analysis of the Coriolis terms is made by setting the right-hand sides of Eq. (5) to zero, along with ϵ and g' , and looking for solutions of the form $e^{\lambda t} e^{-i\omega\Delta t}$. Solving for the absolute frequency ω and exponential growth rate λ we find

$$e^{2\lambda\Delta t} = \frac{1 + (1 - \alpha)^2 \Delta t^2 f^2}{1 + \alpha^2 \Delta t^2 f^2};$$

$$\tan\omega\Delta t = \frac{\Delta t f}{1 - \alpha(1 - \alpha)\Delta t^2 f^2}.$$

We note the following properties. For the system to be stable ($\lambda \leq 0$) to the Coriolis term, it is sufficient that $\alpha \geq 1/2$. For long time steps, the frequency of oscillation, ω , is slowed suggesting that it is useful to damp the motion by using forward weighting ($\alpha > 1/2$). With full forward weighting ($\alpha = 1$) the system is damped at the rate $\lambda = (-1/\Delta t) \log(1 + \Delta t^2 f^2)$. Over the time period f^{-1} , the amplitude of oscillation is multiplied by the damping factor $e^{-\Delta t f/2}$. For large time steps, $\Delta t f \gg 1$, the damping is essentially instantaneous; for intermediate time steps, $\Delta t f \sim 1$, the damping factor is about 60% and even for moderately small time steps, $\Delta t f \sim 1/10$, the damping factor is still 95%.

The consequence of such damping is that the forward weighting in time of the Coriolis terms is a very effective filter of inertial oscillations unless the time step is *extremely* small. For all the timescales of interest and relevance to large-scale oceanography, inertial oscillations will, in practice, be fully filtered. We will now use this implicit damping to eliminate the computational modes from the C–D grid. It should be reiterated that such filtering is not the same as introducing explicit dissipation. Implicit dissipation would dissipate energy from the balanced state whereas the time filtering described here does not. Instead, implicit damping extracts energy only from inertial oscillations and faithfully sustains the balanced state.

4. Numerical results

We now present results from three numerical codes: a C-grid code, an implementation of the C–D scheme, and a B-grid code for comparison. All calculations will use the linear shallow water equations with bottom friction since these are sufficient to expose the issues. The time stepping is identical for all models; implicit backward for the Coriolis term, centered in time for the gravity wave terms, and Euler forward for the bottom friction.

The domain is a flat-bottomed, square basin of depth $H_o = 400$ m, length $L = 4000$ km with solid boundaries on all sides. The Coriolis parameter has a value of f_o

$= 1 \times 10^{-4} \text{ s}^{-1}$ in the middle of the basin and varies linearly with latitude; $\partial f/\partial y = \beta = 1 \times 10^{-11} \text{ s}^{-1} \text{ m}^{-1}$. A zonal wind applies a surface stress of form $\tau^x = \tau_o \sin \pi y/L$, where $-L/2 < y < L/2$ and $\tau_o = 0.2 \text{ N m}^{-2}$ spinning up a single anticyclonic gyre. We choose the reduced gravity to be $g' = 1 \times 10^{-2} \text{ m}^2 \text{ s}^{-1}$ so that the Rossby deformation radius $L_\rho = \sqrt{g'H_o/f_o} = 20$ km. The bottom drag ($\epsilon = 1 \times 10^{-6} \text{ s}^{-1}$) gives a Stommel layer width of $\delta_s = \epsilon/\beta = 100$ km. The time step is $\Delta t = 1728 \text{ s}$ (50 steps per day). The low-resolution calculations (20×20 points) have a grid spacing of $\Delta x = 200$ km so that the Stommel layer is barely resolved but stable, and the wave-resolution $r = 2L_\rho/\Delta x = 0.2$ is small. The high-resolution calculations (200×200 points) have a grid spacing of $\Delta x = 20$ km so that the Stommel layer is well resolved and the wave-resolution $r = 2$ is sufficiently large for qualitatively good behavior on the C-grid.

Figure 6 shows the horizontal divergence field after 100 days of integration from rest for all calculations. The contour interval is $2.5 \times 10^{-9} \text{ s}^{-1}$ and is the same in all plots.

The left column of panels correspond to the C-grid, C–D grid, and B-grid, all at low resolution ($\Delta x = 200$ km), typical of coarsely resolved ocean models. The C-grid (Fig. 6a) exhibits the characteristic gridscale noise anticipated by the analysis of the dispersion relation and is reminiscent of the GCM vertical velocity field (Fig. 1a). The C–D grid (Fig. 6c), by contrast, has no gridscale noise. Further, the solution is very similar to that obtained on the B-grid (Fig. 6e), often the preferred grid at low resolution. It appears, then, that the C–D grid has overcome the difficulties inherent in the C-grid at low resolution.

At high resolution, we believe the C-grid solution (Fig. 6b) to be most accurate. The C–D grid solution (Fig. 6d) is convincingly similar to the C-grid while the B-grid solution (Fig. 6f) exhibits gridscale noise confined to the boundary. These results are all consistent with the analysis.

The numerical results demonstrate that the C–D grid is well behaved in both the low- and high-resolution regimes. However, unlike the B- and C-grids, the C–D grid can be used in either regime. Moreover, the C–D grid is capable of modeling the “gray area” of intermediate resolution ($r \sim 1$ or $\Delta x \sim L_\rho$).

5. Discussion

The development of the C–D grid was motivated by the intolerable level of gridscale noise in the C-grid GCM. Although the noise is generated at boundaries and over topography, its persistence is due to the spatial averaging of the Coriolis terms on the C-grid. We have demonstrated, by analysis and numerical experiments, that this computational spatial mode does not exist on the C–D grid. Insight into how the C–D grid treats the inertia–gravity wave mechanism and the geostrophically

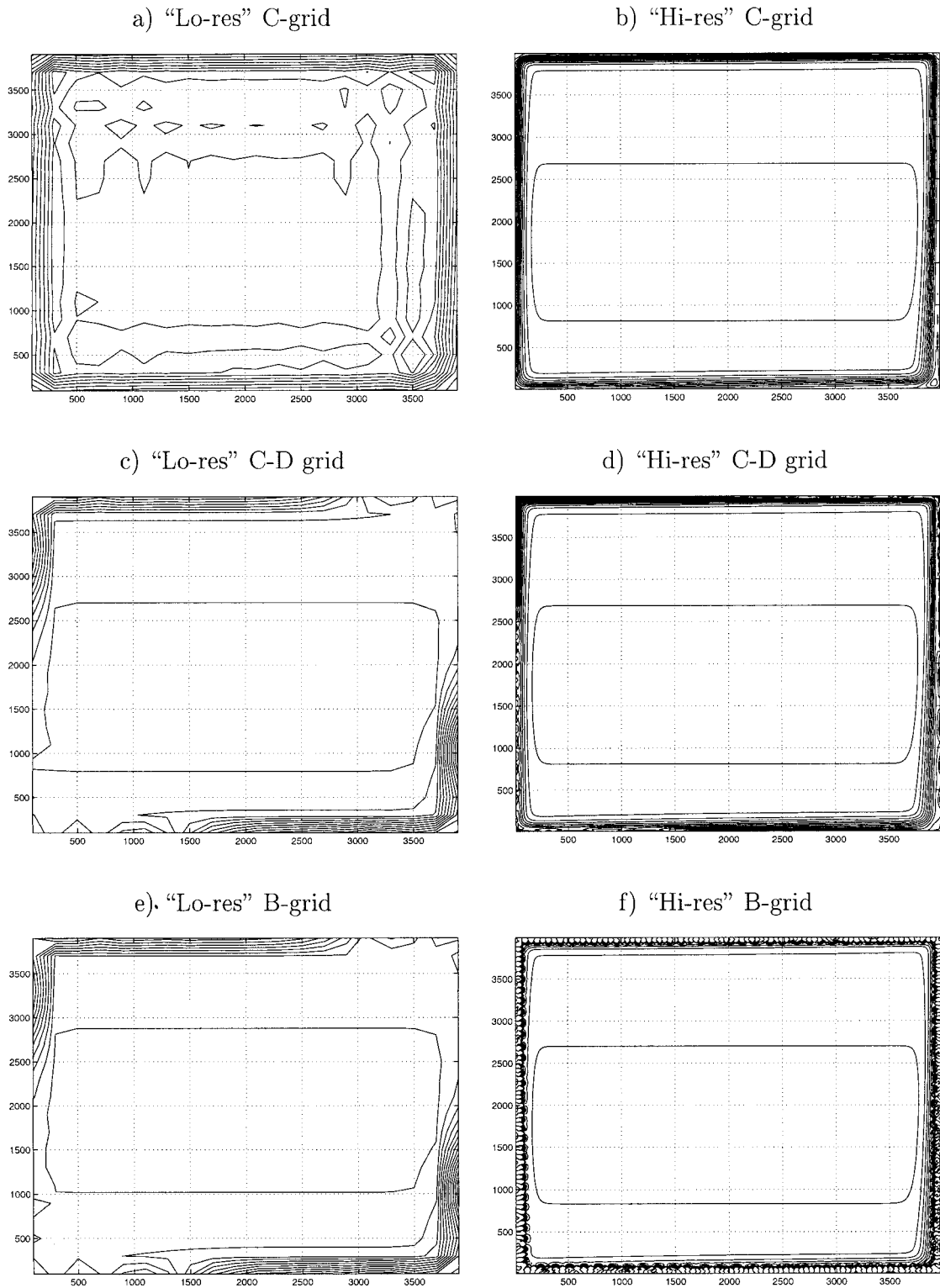


FIG. 6. The divergence field after 100 days of integration for the C-grid, C-D grid, and B-grid models at both high and low resolution. Contour interval is $2.5 \times 10^{-8} \text{ s}^{-1}$.

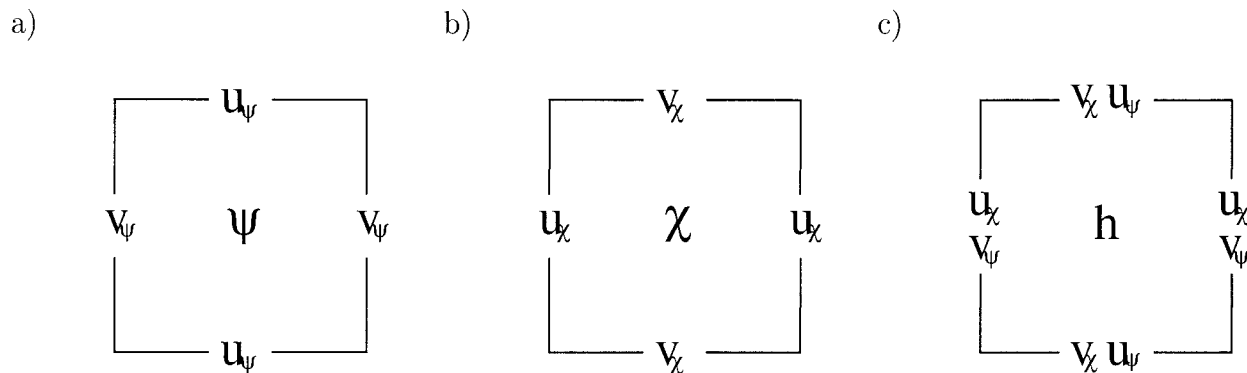


FIG. 7. Breakdown of the Z-grid. The balanced flow (u_ψ, v_ψ) is naturally discretized on (a) the D-grid. The gravity wave dynamics, dominated by the divergent flow (u_χ, v_χ), is naturally discretized on (b) the C-grid. (c) The Z-grid subsequently has well-behaved balanced dynamics and dispersive properties for inertia-gravity waves.

adjusted state can be found by considering how one would place the variables in a prognostic model expressed in terms of vorticity and horizontal divergence

$$\begin{aligned} \frac{\partial}{\partial t} D - f\zeta + g'\nabla^2 h &= \dots & D &= \nabla \cdot \mathbf{u}_\chi \\ \frac{\partial}{\partial t} \zeta + fD &= \dots & \zeta &= \nabla \wedge \mathbf{u}_\psi \\ \frac{\partial}{\partial t} h + HD &= 0. \end{aligned}$$

The natural grid for these equations is shown in Fig. 7. To date, the Z-grid has primarily been used for integrating the balanced equations but Randall (1994) has recently advocated this formulation for discretizing the primitive equations. The Z-grid model does not involve any spatial interpolation and consequently has no computational modes and is prognostic in scalar variables only.¹ The resulting dispersion of inertia-gravity waves and Rossby waves is well behaved and cannot be bettered using second-order finite differencing on any other grid. The Z-grid has not been widely used in the ocean because of the “constant of integration” or boundary condition problem that results from the higher differential order of the system. In short, in multiconnected domains, it is unclear how to determine the transport along channels. Nevertheless, the similarity of aspects of the C–D grid and the Z-grid should be noted. The C–D grid, for moderate time steps, faithfully reproduces gravity wave dynamics because the divergent flow and pressure are positioned on the C-grid. At longer time-scales, the C–D faithfully captures the geostrophically balanced flow because the rotational components of ve-

locity are positioned on the D-grid with respect to the pressure.

The continuity equation only makes use of the C-grid quantities so we have been tempted to think of the C–D grid as an augmented C-grid. This is probably inappropriate since the D-grid equations do represent half the kinetic energy of the system. In the context of a more comprehensive model, the D-grid velocities could be used in evaluating other terms such as momentum advection though we have not yet tried this. The principle disadvantage of the C–D grid is the doubling of resolution in velocity but not in pressure; the effective resolution of the model is the coarsest of the two.

We have chosen not to include the nonlinear terms here, so that the linear nature of the C-grid noise issue would be exposed. The gravity wave dynamics are largely controlled by the C-grid. The D-grid momentum equations are stepped forward by interpolating the forcing and pressure terms to the appropriate positions. The D-grid equations are, therefore, predominantly diagnostic, by virtue of the implicit backward time stepping of the Coriolis terms. The potential decoupling of the C- and D-grid velocities is avoided by the implicit treatment of the Coriolis terms. At the equator, the vanishing of f renders the Coriolis terms small so we expect that the D-grid velocities would play no role in the model.

There are no apparent benefits to the C–D grid at high resolution so we do not advocate the C–D grid in high-resolution, “eddy-resolving” studies. The C-grid only needs to be augmented at low spatial resolutions. Our intent here has been to show that we can successfully avoid gridscale noise difficulties in a low-resolution C-grid model without introducing scale-selective dissipation. Instead, we have used the time-filtering properties of an implicit time-stepping scheme to filter the fast computational modes on the C–D grid.

Acknowledgments. We wish to thank an anonymous reviewer and Ernst Maier-Reimer for their helpful comments on this note. We are grateful for financial support

¹ There are difficulties in discretizing vector equations. The evolution of scalar quantities, as described here, can be written as the divergence of a flux that translates very well to the Eulerian nature of fixed grid models and is also very suitable for other discretization techniques such as finite element and finite volume methods.

from the National Science Foundation, NSF-OCE-9819488, and the American Automobile Manufacturers Association.

REFERENCES

- Arakawa, A., and V. R. Lamb, 1977: Computational design of the basic dynamical processes of the UCLA general circulation model. *Methods in Computational Physics*, J. Chang, Ed., Academic Press, 174–267.
- Blanke, B., and P. Delecluse, 1993: Variability of the tropical Atlantic Ocean simulated by a general circulation model with two different mixed-layer physics. *J. Phys. Oceanogr.*, **23**, 1363–1388.
- Bryan, K., 1969: A numerical method for the study of the circulation of the World Ocean. *J. Comput. Phys.*, **4**, 347–376.
- Fox-Rabinovitz, M. S., 1991: Computational dispersion of horizontal staggered grids for atmospheric and ocean models. *Mon. Wea. Rev.*, **119**, 1624–1639.
- Haidvogel, D. B., J. Wilkin, and R. Young, 1991: A semi-spectral primitive equation ocean circulation model using sigma and orthogonal curvilinear coordinates. *J. Comput. Phys.*, **94**, 151–185.
- Marshall, J., A. Adcroft, C. Hill, L. Perelman, and C. Heisey, 1997: A finite-volume, incompressible Navier-Stokes model for studies of the ocean on parallel computers. *J. Geophys. Res.*, **102** (C3), 5733–5752.
- Mesinger, F., and A. Arakawa, 1976: Numerical methods used in atmospheric models. Tech. Rep., WMO/ICSU Joint Organizing Committee GARP Publ. Series.
- Randall, D. A., 1994: Geostrophic adjustment and the finite-difference shallow water equations. *Mon. Wea. Rev.*, **122**, 1371–1377.
- Smith, L. T., D. B. Boudra, and R. Bleck, 1990: A wind-driven isopycnal coordinate model of the north and equatorial Atlantic Ocean. 2: The Atlantic-basin experiments. *J. Geophys. Res.*, **95** (C8), 13 105–13 128.
- Wajsovicz, R. C., 1986a: Adjustment of the ocean under buoyancy forces. Part II: The role of planetary waves. *J. Phys. Oceanogr.*, **16**, 2115–2136.
- , 1986b: Free planetary waves in finite-difference numerical models. *J. Phys. Oceanogr.*, **16**, 773–789.
- , and A. Gill, 1986: Adjustment of the ocean under buoyancy forces. Part I: The role of Kelvin waves. *J. Phys. Oceanogr.*, **16**, 2097–2114.